

Supplementary Material: A weak additivity principle for current statistics in d -dimensions

C. Pérez-Espigares,¹ P.L. Garrido,² and P.I. Hurtado²

¹*University of Modena and Reggio Emilia, via G. Campi 213/b, 41125 Modena, Italy*

²*Institute Carlos I for Theoretical and Computational Physics,*

and Departamento de Electromagnetismo y Física de la Materia, Universidad de Granada, 18071 Granada, Spain
(Dated: March 28, 2016)

PACS numbers: 05.40.-a, 05.70.Ln, 74.40.Gh, 02.50.-r, 44.10.+i

Appendix A: Quantum Hamiltonian formalism for the current statistics of the $2d$ ZRP

In this appendix we derive in a self-contained way the current statistics of the $2d$ Zero-Range Process (ZRP) using the quantum Hamiltonian formalism for the master equation as main tool. In particular, we follow Ref. [1] where a similar calculation has been recently presented. Our aim is to calculate the current scaled cumulant generating function $\mu_L(\boldsymbol{\lambda})$ and the microscopic optimal density profiles associated to a given current fluctuation in a system of linear size L . Within the quantum Hamiltonian formalism, the master equation is written in Schrödinger form [2, 3] as

$$\frac{d|P\rangle}{dt} = -H|P\rangle, \quad (\text{A1})$$

with the so-called *Hamiltonian* H given by the stochastic generator containing the transition rates between all states of the system. We have introduced Dirac's bra and ket notation, with the ket $|P\rangle$ representing the probability column vector $(P(C_1), P(C_2), \dots)^T$, with T denoting transposition, and where $P(C_k)$ denotes the probability measure on the set of all configurations $C_k = (n_1, n_2, \dots, n_M)$, $n_i \in \mathbb{N}$, being n_i the number of particles on site i (out of a total number of M sites). The probability vector is then defined as $|P\rangle = \sum_k P(C_k)|C_k\rangle$ where $|C_k\rangle$ is a basis vector for the particle configuration, i.e. it corresponds to the column vector $|C_k\rangle = (0, 0, \dots, 0, 1, 0, \dots)^T$ with all components equal to zero except for the component corresponding to configuration C_k . The probability vector is normalized such that $\langle 1|P\rangle = 1$ where $\langle 1| = \sum_k \langle C_k|$ is the row vector with all elements equal to one and $\langle C|C'\rangle = \delta_{CC'}$. One can readily verify that $\langle 1|$ is the left-eigenvector of H with zero eigenvalue $\langle 1|H = 0$ (expressing conservation of probability). On the other hand, the stationary distribution or *ground state* of the stochastic process, denoted here as $|P^*\rangle$, corresponds to the right-eigenvector of H with zero eigenvalue

$$H|P^*\rangle = 0. \quad (\text{A2})$$

The $2d$ ZRP we consider here is defined on a square lattice of linear size L with particle reservoirs at the boundaries in the x -direction and with periodic boundary conditions in the y -direction. Configurations are denoted as $C_k = (n_{11}, n_{12}, \dots, n_{LL})$, $n_{ji} \in \mathbb{N}$, $j, i \in [1, L]$, being n_{ji} the number of particles on site (j, i) . Notice that for each site in the square lattice, j denotes the row index while i denotes the column. The dynamics is as follows: In the bulk, particles jump to randomly chosen nearest neighbors at a rate $\omega_\alpha(n_{ji}) = h_\alpha f(n_{ji})$, with $f(n_{ji})$ the interaction function (which depends only on the population of the departure site) and h_α the (constant) hopping rate along the α -direction (x or y -direction). In addition, particles are injected at rate α (and removed at rate γ) at the left boundary -corresponding to the first column of sites- and injected at rate δ (and removed at rate β) at the right boundary -corresponding to the last column. Notice that anisotropy can be modeled in this model by considering $h_x \neq h_y$.

As for the one dimensional ZRP with open boundaries [4], the stationary distribution is given by a product measure

$$|P^*\rangle = |P_{1,1}^*\rangle \otimes |P_{1,2}^*\rangle \otimes \dots \otimes |P_{L,L}^*\rangle \quad (\text{A3})$$

where $|P_{j,i}^*\rangle$ is the probability vector corresponding to the marginal distribution for the site (j, i) , i.e. $|P_{j,i}^*\rangle = \sum_{n_{ji}} P_{j,i}^*(n_{ji})|n_{ji}\rangle$, whose components correspond to the probability of finding n_{ji} particles on site (j, i) :

$$P_{j,i}^*(n_{ji}) = \frac{z_{j,i}^{n_{ji}}}{Z_{j,i}} \prod_{k=1}^{n_{ji}} f(k)^{-1}. \quad (\text{A4})$$

Here $z_{j,i}$ is the fugacity of site (j, i) and $Z_{j,i}$ is the local analogue of the grand-canonical partition function

$$Z_{j,i} \equiv Z(z_{j,i}) = \sum_{n=0}^{\infty} z_{j,i}^n \prod_{k=1}^n f(k)^{-1}. \quad (\text{A5})$$

It is important to note that the convergence of the partition function depends on how we choose the interaction function $f(k)$. In this work, we restrict to the ZRP in the fluid regime (i.e. in the absence of condensation), so for the $f(k)$'s chosen (either constant or proportional to the number of particles) we consider below current fluctuations within the radius of convergence of (A5). In order to relate the fugacity and the mean density on site (j, i) , we introduce now the local particle number operator as the diagonal matrix \hat{n}_{ji} with diagonal elements n_{ji} . Notice that \hat{n}_{ji} acts exclusively on the $(j, i)^{th}$ component of the configuration vector. Then by using (A4) and (A5), we find

$$\rho_{j,i} \equiv \langle n_{ji} \rangle = \langle 1 | \hat{n}_{ji} | P^* \rangle = \sum_{n_{ji}=0}^{\infty} n_{ji} P_{j,i}^*(n_{ji}) = z_{j,i} \frac{\partial \log Z_{j,i}}{\partial z_{j,i}}. \quad (\text{A6})$$

In order to write explicitly the Hamiltonian of the 2d ZRP, we introduce now the following ladder and diagonal operators,

$$a_{ji}^+ = \begin{pmatrix} 0 & 0 & 0 & 0 & \cdots \\ 1 & 0 & 0 & 0 & \cdots \\ 0 & 1 & 0 & 0 & \cdots \\ 0 & 0 & 1 & 0 & \cdots \\ \cdots & \cdots & \cdots & \cdots & \cdots \end{pmatrix}, \quad a_{ji}^- = \begin{pmatrix} 0 & f(1) & 0 & 0 & \cdots \\ 0 & 0 & f(2) & 0 & \cdots \\ 0 & 0 & 0 & f(3) & \cdots \\ 0 & 0 & 0 & 0 & \cdots \\ \cdots & \cdots & \cdots & \cdots & \cdots \end{pmatrix} \quad d_{ji} = \begin{pmatrix} 0 & 0 & 0 & 0 & \cdots \\ 0 & f(1) & 0 & 0 & \cdots \\ 0 & 0 & f(2) & 0 & \cdots \\ 0 & 0 & 0 & f(3) & \cdots \\ \cdots & \cdots & \cdots & \cdots & \cdots \end{pmatrix} \quad (\text{A7})$$

The subscript (j, i) indicates that the respective matrix acts non-trivially only on site (j, i) of the lattice, and as a unit operator on all other sites. In this way, the Hamiltonian of the 2d ZRP in a square lattice reads [1]

$$\begin{aligned} -H = & \sum_{j=1}^L \left\{ \alpha(a_{j,1}^+ - 1) + \gamma(a_{j,1}^- - d_{j,1}) + \delta(a_{j,L}^+ - 1) + \beta(a_{j,L}^- - d_{j,L}) \right. \\ & + \sum_{i=1}^{L-1} h_x(a_{j,i}^- a_{j,i+1}^+ - d_{j,i}) + h_x(a_{j,i}^+ a_{j,i+1}^- - d_{j,i+1}) \\ & \left. + \sum_{i=1}^L h_y(a_{j,i}^- a_{j+1,i}^+ - d_{j,i}) + h_y(a_{j,i}^+ a_{j+1,i}^- - d_{j+1,i}) \right\}, \quad (\text{A8}) \end{aligned}$$

Note that, due to the periodic boundary conditions along the y -direction, we identify $j = L + 1$ with $j = 1$. The first line of the r.h.s of the above equation reflects the injection and extraction of particles from the boundary reservoirs, i.e. it corresponds to the boundary pairs in the first and last column. The second and the third lines correspond to the interaction of the $L(L - 1)$ horizontal and the L^2 vertical bulk pairs, respectively.

1. Current fluctuations for the 2d ZRP

Our first task is to define the microscopic space&time-integrated current \mathbf{q} in the bulk of the lattice during a given observation time interval $[0, t]$. In few words, every time a particle jumps between two bulk neighboring sites along the α -direction, $\alpha = x, y$, we add or subtract one to the corresponding α -component of the integrated current. In this way, the space&time-averaged current vector is defined as

$$\mathbf{q} = \frac{1}{t} \left(\frac{1}{L-1} (Q_t^{+,x} - Q_t^{-,x}), \frac{1}{L} (Q_t^{+,y} - Q_t^{-,y}) \right) \quad (\text{A9})$$

where $Q_t^{\pm,\alpha}$ are the total number of particle jumps in the $\pm\alpha$ -direction, $\alpha = x, y$, in a given microscopic time interval $[0, t]$. Recall that as we are considering the contributions of all the bulk pairs we have to divide the current by $(L-1)$ if the jump occurs in the x -direction or by L if it occurs in the y -direction in order to count the number of particles that traverses the system per unit *area* and unit time. The empirical averaged current obeys a large deviation principle with large deviation function

$$G_L(\mathbf{q}) = \lim_{t \rightarrow \infty} \frac{1}{t} \log P(\mathbf{q}), \quad (\text{A10})$$

and its scaled cumulant generating function (SCGF) is defined as

$$\mu_L(\boldsymbol{\lambda}) = \lim_{t \rightarrow \infty} \frac{1}{t} \log \langle e^{t\boldsymbol{\lambda} \cdot \mathbf{q}} \rangle. \quad (\text{A11})$$

It is then easy to show [5] that the SCGF is linked to the spectral properties of a modified or tilted Hamiltonian \hat{H} . In particular, $\langle e^{t\lambda \cdot \mathbf{q}} \rangle = \langle e^{-\hat{H}t} \rangle$, where the new operator \hat{H} is obtained by multiplying the terms of H corresponding to bulk particle transitions by $e^{\pm\lambda_x/(L-1)}$ for jumps in the $\pm x$ -direction and by $e^{\pm\lambda_y/L}$ for jumps in the $\pm y$ -direction. This modified Hamiltonian hence reads

$$\begin{aligned} -\hat{H} &= \sum_{j=1}^L \left\{ \alpha(a_{j,1}^+ - 1) + \gamma(a_{j,1}^- - d_{j,1}) + \delta(a_{j,L}^+ - 1) + \beta(a_{j,L}^- - d_{j,L}) \right. \\ &\quad + \sum_{i=1}^{L-1} h_x(e^{\frac{\lambda_x}{L-1}} a_{j,i}^- a_{j,i+1}^+ - d_{j,i}) + h_x(e^{\frac{-\lambda_x}{L-1}} a_{j,i}^+ a_{j,i+1}^- - d_{j,i+1}) \\ &\quad \left. + \sum_{i=1}^L h_y(e^{\frac{\lambda_y}{L}} a_{j,i}^- a_{j+1,i}^+ - d_{j,i}) + h_y(e^{\frac{-\lambda_y}{L}} a_{j,i}^+ a_{j+1,i}^- - d_{j+1,i}) \right\}. \end{aligned} \quad (\text{A12})$$

Now, assuming that the spectrum of \hat{H} is gapped and introducing the associated spectral decomposition, we can write

$$\langle e^{t\lambda \cdot \mathbf{q}} \rangle = \langle 1|e^{-\hat{H}t}|P_0 \rangle = \sum_k \langle 1|\phi_k \rangle \langle \phi_k|P_0 \rangle e^{-\epsilon_k(\lambda)t} \xrightarrow{t \gg 1} \langle 1|\psi \rangle \langle \psi|P_0 \rangle e^{-\epsilon_0(\lambda)t} \quad (\text{A13})$$

where $|\psi \rangle$ and $\langle \psi|$ are the right and left eigenvectors of \hat{H} associated with the lowest eigenvalue $\epsilon_0(\lambda)$, and $|P_0 \rangle$ is an arbitrary specific initial particle distribution obeying the normalization condition $\langle 1|P_0 \rangle = 1$. If all prefactors in (A13) are finite (i.e. if $\langle 1|\psi \rangle$, $\langle \psi|P_0 \rangle$ and $\langle \psi|\psi \rangle$ are finite) one finds, by using (A11) and (A13), that

$$\mu_L(\lambda) = -\epsilon_0(\lambda). \quad (\text{A14})$$

To compute $\epsilon_0(\lambda)$, we assume that the unnormalized right eigenvector has a product form similar to (A3), i.e.,

$$|\psi \rangle = |\psi_{1,1} \rangle \otimes |\psi_{1,2} \rangle \otimes \cdots \otimes |\psi_{L,L} \rangle \quad (\text{A15})$$

where $|\psi_{j,i} \rangle$ is the vector for the (j,i) -site, i.e., $|\psi_{j,i} \rangle = \sum_{n_{j,i}} \psi_{j,i}^{\text{right}}(n_{j,i}) |n_{j,i} \rangle$, whose components are $\psi_{j,i}^{\text{right}}(n_{j,i}) = \hat{z}_{j,i}^{n_{j,i}} \prod_{k=1}^{n_{j,i}} f(k)^{-1}$ with $\hat{z}_{j,i}$ some modified fugacities still unknown. With the product form (A15) one can readily check that

$$a_{j,i}^+ |\psi \rangle = \hat{z}_{j,i}^{-1} d_{j,i} |\psi \rangle, \quad (\text{A16})$$

$$a_{j,i}^- |\psi \rangle = \hat{z}_{j,i} |\psi \rangle. \quad (\text{A17})$$

Using these equations we get that

$$\begin{aligned} -\hat{H}|\psi \rangle &= \sum_{j=1}^L \left\{ -(\alpha + \delta - (\gamma \hat{z}_{j,1} + \beta \hat{z}_{j,L})) \right. \\ &\quad + \sum_{i=2}^{L-1} \hat{z}_{j,i}^{-1} d_{j,i} \left[\hat{z}_{j,i+1} h_x e^{\frac{-\lambda_x}{L-1}} - \hat{z}_{j,i} (2h_x + h_y (1 - e^{\frac{\lambda_y}{L}}) + h_y (1 - e^{\frac{-\lambda_y}{L}})) + \hat{z}_{j,i-1} h_x e^{\frac{\lambda_x}{L-1}} \right] \\ &\quad + \hat{z}_{j,1}^{-1} d_{j,1} \left(\hat{z}_{j,2} h_x e^{\frac{-\lambda_x}{L-1}} - \hat{z}_{j,1} (h_x + \gamma + h_y (1 - e^{\frac{\lambda_y}{L}}) + h_y (1 - e^{\frac{-\lambda_y}{L}})) + \alpha \right) \\ &\quad \left. + \hat{z}_{j,L}^{-1} d_{j,L} \left(\hat{z}_{j,L-1} h_x e^{\frac{\lambda_x}{L-1}} - \hat{z}_{j,L} (\beta + h_x + h_y (1 - e^{\frac{\lambda_y}{L}}) + h_y (1 - e^{\frac{-\lambda_y}{L}})) + \delta \right) \right\} |\psi \rangle. \end{aligned} \quad (\text{A18})$$

It is clear that if $|\psi \rangle$ is a right eigenvector, the coefficients that multiply the matrix d must vanish. In this way, we can compute the components of the right eigenvector fugacities by solving the following recurrence relation

$$\hat{z}_{i+1} h_x e^{\frac{-\lambda_x}{L-1}} - \hat{z}_i (2h_x + h_y (1 - e^{\frac{\lambda_y}{L}}) + h_y (1 - e^{\frac{-\lambda_y}{L}})) + \hat{z}_{i-1} h_x e^{\frac{\lambda_x}{L-1}} = 0 \quad (\text{A19})$$

with boundary conditions

$$\hat{z}_2 h_x e^{\frac{-\lambda_x}{L-1}} - \hat{z}_1 (h_x + \gamma + h_y (1 - e^{\frac{\lambda_y}{L}}) + h_y (1 - e^{\frac{-\lambda_y}{L}})) + \alpha = 0 \quad (\text{A20})$$

$$\hat{z}_{L-1} h_x e^{\frac{\lambda_x}{L-1}} - \hat{z}_L (\beta + h_x + h_y (1 - e^{\frac{\lambda_y}{L}}) + h_y (1 - e^{-\frac{\lambda_y}{L}})) + \delta = 0. \quad (\text{A21})$$

Notice that in the previous equations we have made use of the periodic boundary conditions to argue that fugacities are invariant in the y -direction, $\hat{z}_{j,i} = \hat{z}_i, \forall j$. Equations (A19)-(A21) can be solved exactly with a computer to get the fugacity of the right eigenvector for each column \hat{z}_i ($i \in [1, L]$), but the expressions obtained are too cumbersome to write them explicitly here. Thus, from eqs. (A18)-(A21), we get the lowest eigenvalue of \hat{H}

$$\hat{H}|\psi\rangle = L\left(\alpha + \delta - (\gamma\hat{z}_1 + \beta\hat{z}_L)\right)|\psi\rangle = \epsilon_0(\boldsymbol{\lambda})|\psi\rangle, \quad (\text{A22})$$

from which that SCGF in (A14) follows as

$$\mu_L(\boldsymbol{\lambda}) = -L\left(\alpha + \delta - (\gamma\hat{z}_1 + \beta\hat{z}_L)\right), \quad (\text{A23})$$

with $\hat{z}_{1,L}$ explicitly given in terms of the solution of recurrence (A19)-(A21).

2. Microscopic optimal density profiles for the 2d ZRP

In order to compute the mean density in each site, we need both the right and left dominant eigenvectors associated to a given current fluctuation. For the left eigenvector, we assume again a product form similar to eq. (A15), i.e [5]

$$\langle\psi| = (\psi_{1,1}| \otimes (\psi_{1,2}| \otimes \cdots \otimes (\psi_{L,L}| \quad (\text{A24})$$

where $(\psi_{j,i}|$ is the vector for the (j, i) -site, i.e, $(\psi_{j,i}| = \sum_{n_{j,i}} \psi_{j,i}^{\text{left}}(n_{j,i})|n_{j,i}\rangle$, whose components are $\psi_{j,i}^{\text{left}}(n_{j,i}) = \tilde{z}_{j,i}^{n_{j,i}}$ with $\tilde{z}_{j,i}$ some modified fugacities to be determined below. With the product form (A24) one can readily check that

$$\langle\psi|a_{j,i}^+ = \langle\psi|\tilde{z}_{j,i}, \quad (\text{A25})$$

$$\langle\psi|a_{j,i}^- = \langle\psi|\tilde{z}_{j,i}^{-1}d_{j,i}. \quad (\text{A26})$$

Using these equations we get that

$$\begin{aligned} -\langle\psi|\hat{H} = \langle\psi| \sum_{j=1}^L \left\{ -(\alpha + \delta - (\alpha\tilde{z}_{j,1} + \delta\tilde{z}_{j,L})) \right. \\ + \sum_{i=2}^{L-1} \tilde{z}_{j,i}^{-1}d_{j,i} \left[\tilde{z}_{j,i+1}h_x e^{\frac{\lambda_x}{L-1}} - \tilde{z}_{j,i}(h_x + h_x + h_y(1 - e^{\frac{\lambda_y}{L}}) + h_y(1 - e^{-\frac{\lambda_y}{L}})) + \tilde{z}_{j,i-1}h_x e^{\frac{-\lambda_x}{L-1}} \right] \\ + \tilde{z}_{j,1}^{-1}d_{j,1} \left(\tilde{z}_{j,2}h_x e^{\frac{\lambda_x}{L-1}} - \tilde{z}_{j,1}(h_x + \gamma + h_y(1 - e^{\frac{\lambda_y}{L}}) + h_y(1 - e^{-\frac{\lambda_y}{L}})) + \gamma \right) \\ \left. + \tilde{z}_{j,L}^{-1}d_{j,L} \left(\tilde{z}_{j,L-1}h_x e^{\frac{-\lambda_x}{L-1}} - \tilde{z}_{j,L}(\beta + h_x + h_y(1 - e^{\frac{\lambda_y}{L}}) + h_y(1 - e^{-\frac{\lambda_y}{L}})) + \beta \right) \right\}. \end{aligned} \quad (\text{A27})$$

As before, the coefficients multiplying matrix d must vanish, resulting in the following recurrence relation for the left eigenvector fugacities (where we have considered again that $\tilde{z}_{j,i} = \tilde{z}_i, \forall j$)

$$\tilde{z}_{i+1}h_x e^{\frac{\lambda_x}{L-1}} - \tilde{z}_i(2h_x + h_y(1 - e^{\frac{\lambda_y}{L}}) + h_y(1 - e^{-\frac{\lambda_y}{L}})) + \tilde{z}_{i-1}h_x e^{\frac{-\lambda_x}{L-1}} = 0 \quad (\text{A28})$$

with boundary conditions

$$\tilde{z}_2h_x e^{\frac{\lambda_x}{L-1}} - \tilde{z}_1(h_x + \gamma + h_y(1 - e^{\frac{\lambda_y}{L}}) + h_y(1 - e^{-\frac{\lambda_y}{L}})) + \gamma = 0 \quad (\text{A29})$$

$$\tilde{z}_{L-1}h_x e^{\frac{-\lambda_x}{L-1}} - \tilde{z}_L(\beta + h_x + h_y(1 - e^{\frac{\lambda_y}{L}}) + h_y(1 - e^{-\frac{\lambda_y}{L}})) + \beta = 0. \quad (\text{A30})$$

By solving eqs. (A28)-(A30) we get the fugacity of the left eigenvector for each column, \tilde{z}_i ($i \in [1, L]$). Moreover, the SCGF can be equivalently written in terms of these fugacities as

$$\mu_L(\boldsymbol{\lambda}) = -L\left(\alpha + \delta - (\alpha\tilde{z}_1 + \delta\tilde{z}_L)\right). \quad (\text{A31})$$

One can check that as $\lambda \rightarrow 0$, $\langle \psi | \rightarrow \langle 1 |$, $|\psi\rangle \rightarrow |P^*\rangle$ and $\mu_L(\lambda) \rightarrow 0$, as expected. Finally, we can compute the microscopic optimal profiles associated to a current fluctuation (parametrized via λ) by averaging the mean occupation number in each column i over the right and left dominant eigenvectors, once normalized, i.e.

$$\rho_{j,i} \equiv \langle n_{ji} \rangle = \frac{\langle \psi | \hat{n}_{ji} | \psi \rangle}{\langle \psi | \psi \rangle} = \frac{(\bar{z}_i \hat{z}_i)^{n_{ji}} \prod_{k=1}^{n_{ji}} f(k)^{-1}}{\sum_{n_{ji}=0}^{\infty} (\bar{z}_i \hat{z}_i)^{n_{ji}} \prod_{k=1}^{n_{ji}} f(k)^{-1}} = \bar{z}_i \frac{\partial \log \bar{Z}_i}{\partial \bar{z}_i} \quad (\text{A32})$$

where $\bar{z}_i \equiv \bar{z}_i \hat{z}_i$ and

$$\bar{Z}_i \equiv \sum_{n=0}^{\infty} \bar{z}_i^n \prod_{k=1}^n f(k)^{-1}. \quad (\text{A33})$$

As expected, the mean occupation number on site (j, i) just depends on \bar{z}_i , so the microscopic density profile associated to a given current fluctuation exhibits structure only along the gradient direction, in agreement with general MFT predictions in the main text.

On the other hand, in this work we consider two different interaction functions $f(k)$. The first one is a constant $f(k) = 1$, and corresponds to a $2d$ ZRP with effective attractive interaction between particles at each lattice site. The associated optimal density profile is

$$\rho_i = \frac{\bar{z}_i}{1 - \bar{z}_i}. \quad (\text{A34})$$

In this case, the reservoir fugacities in terms of the injection and extraction rate are given by $z_1 = \alpha/\gamma$ and $z_L = \delta/\beta$ and the reservoirs densities by $\rho_L = \frac{\alpha/\gamma}{1-\alpha/\gamma}$ and $\rho_R = \frac{\delta/\beta}{1-\delta/\beta}$. The parameters chosen in the main text for the isotropic ZRP case (with $h_x = 1/2$, $h_y = 1/2$), whose results are displayed in Fig. ?? and Fig. 2, are $\alpha = 1/4$, $\gamma = 1/2$, $\delta = 1/22$ and $\beta = 1/2$. These parameters correspond to $\rho_L = 1$ and $\rho_R = 0.1$. The same parameters are chosen for the anisotropic ZRP case studied in Appendix B (with $h_x = 1/2$, $h_y = 1$), see Fig. 1 there. The second interaction function that we consider is $f(k) = k$ and corresponds to a $2d$ fluid of independent random walkers (RW), giving rise to the following optimal microscopic density profile

$$\rho_i = \bar{z}_i. \quad (\text{A35})$$

The reservoirs fugacities are given by $z_1 = \alpha/\gamma$ and $z_L = \delta/\beta$, and the reservoirs densities are now $\rho_L = \alpha/\gamma$ and $\rho_R = \delta/\beta$. The parameters chosen in the isotropic RW case studied in Appendix B (with $h_x = 1/2$, $h_y = 1/2$), see Fig. 3, are $\alpha = 1$, $\gamma = 1/2$, $\delta = 1$, $\beta = 1$, which correspond to $\rho_L = 2$ and $\rho_R = 1$.

3. Comparing microscopic and macroscopic results

In order to compare the previous microscopic results above with macroscopic fluctuation theory predictions we need to perform a diffusive scaling on the microscopic results. This consists in the following transformations of space and time: $x = i/L$, $y = j/L$ and $\tau = t/L^2$, where i, j, t are the microscopic space and time variables and x, y and τ the macroscopic ones. Applying this diffusive scaling, the macroscopic SCGF reads

$$\mu(\lambda) = \lim_{L \rightarrow \infty} \frac{\mu_L(\lambda)}{L^{d-2}}. \quad (\text{A36})$$

Therefore, in $d = 2$ we have $\mu(\lambda) = \lim_{L \rightarrow \infty} \mu_L(\lambda)$, with $\mu_L(\lambda)$ given by eq. (A23). Then for every $\lambda^* = (\lambda_x^*, \lambda_y^*)$ we can calculate the current large deviation function knowing that

$$G(\mathbf{J}) = \max_{\lambda} [\mu(\lambda) - \lambda \cdot \mathbf{J}] = \mu(\lambda^*) - \lambda^* \cdot \mathbf{J} \quad (\text{A37})$$

where $\mathbf{J} = (J_x, J_y) = \left(\frac{\partial \mu(\lambda)}{\partial \lambda_x} \Big|_{\lambda=\lambda^*}, \frac{\partial \mu(\lambda)}{\partial \lambda_y} \Big|_{\lambda=\lambda^*} \right)$. Finally, the optimal macroscopic profile $\rho(x)$ (with $x \in [0, 1]$) is nothing but the microscopic optimal profile ρ_i with $x = \frac{i}{L}$ and ρ_i given by eqs. (A34) or (A35) depending on the interaction function at play. As a crosscheck of our results, note that the macroscopic and microscopic optimal profiles obtained for the ZRP with $f(k) = 1$ for the angles $\phi = 0, \pi$ are the same of those obtained in Ref. [6] for the one-dimensional symmetric case.

Appendix B: Some additional results

In this Appendix we provide additional data which support our conclusions in the main text. In particular, we report further exact microscopic results obtained by applying the quantum Hamiltonian formalism of Appendix A to the Zero Range Process (ZRP) described in the main text [?], both in the isotropic and anisotropic cases, and to a fluid of random walkers (RW model).

We first focus on the effect of anisotropy on the current LDF and the associated optimal density profiles. Fig. 1 shows $G(\mathbf{J})$ (top) and the optimal density profiles $\bar{\rho}(x; \mathbf{J})$ (bottom, after subtracting the steady-state profile $\rho_{\text{av}}(x)$) for the anisotropic ZRP with jump rates ($h_x = 1/2, h_y = 1$), $L = 10^5$, and boundary densities $\rho_L = 1$ and $\rho_R = 0.1$. Similarly to the results in the main text, wAP predictions perfectly fit the exact microscopic results derived within the matrix approach of Appendix A. On the other hand, theoretical curves based on the sAP fail to correctly predict the shape of $G(\mathbf{J})$ and the associated optimal density profiles, except

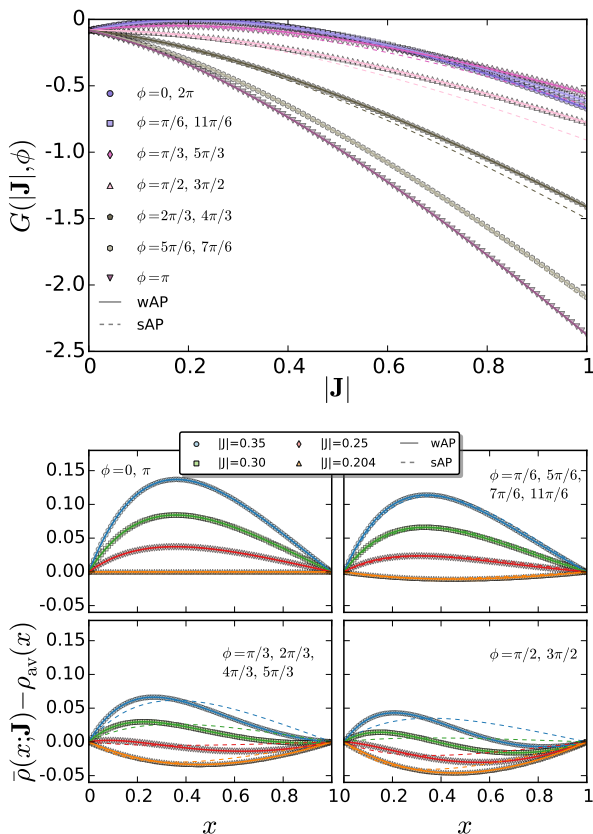


FIG. 1. (Color online) Top: Current LDF for the *anisotropic* ZRP ($h_x = 1/2, h_y = 1$) with $\rho_L = 1$ and $\rho_R = 0.1$, as a function of $|\mathbf{J}|$ for different angles $\phi = \tan^{-1}(J_y/J_x)$. Bottom: Excess optimal density profiles for different $|\mathbf{J}|$ and ϕ . Symbols stand for exact matrix computations for $L = 10^5$, while solid (dashed) lines represent wAP (sAP) predictions.

for currents $\mathbf{J} = (J_{\parallel}, 0)$ aligned with the gradient direction, where both wAP and sAP predictions converge as proven in the main text. In any case, it is interesting to note that optimal density profiles responsible of a given current fluctuation \mathbf{J} are typically different from the average, steady-state density profile, see bottom panel in Fig. 1. This general observation, common to all studied models, stems from the (typically nonlinear) dependence of the diffusivity and mobility transport coefficients on the local density field.

The power of the quantum Hamiltonian formalism for the master equation, when combined with the factorization property of the ZRP [7], allows us to study its current statistics not only for very large lattice linear sizes $L = 10^5$, but also to understand the role of finite-size corrections from a microscopic point of view. We exploit now this possibility in order to compare the finite-size behavior of the ZRP with the more complex KMP model studied in the main text [8], for which reliable data for current statistics can be obtained only for relatively small system sizes via rare-event Monte Carlo simulation techniques [9–13]. Fig. 2 shows for the isotropic ZRP ($h_x = 1/2, h_y = 1/2$) the Legendre-Fenchel transform of the current LDF,

$$\mu(\boldsymbol{\lambda}) = \max_{\mathbf{J}} [G(\mathbf{J}) + \boldsymbol{\lambda} \cdot \mathbf{J}],$$

for a fixed value of $z = |\mathbf{z}|$, with $\mathbf{z} \equiv \boldsymbol{\lambda} + \boldsymbol{\epsilon}$ and $\boldsymbol{\epsilon} = \frac{1}{2} \ln[\rho_L(1 + \rho_R)/(\rho_R(1 + \rho_L))]$, as a function of the current angle $\phi = \tan^{-1}(J_y/J_x)$ for $\rho_L = 1, \rho_R = 0.1$, and increasing values of L , together with the wAP and sAP predictions. As described in the main text, while sAP predicts no angular dependence for $\mu(\boldsymbol{\lambda})$, the wAP does predicts a double-bump structure, which is fully

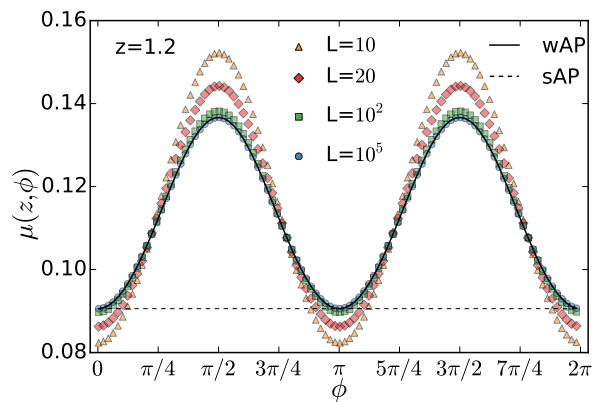


FIG. 2. (Color online) Legendre transform of the current LDF of the isotropic ZRP ($h_x = 1/2, h_y = 1/2$) as a function of ϕ for $z \equiv |\mathbf{z}| = 1.2, \rho_L = 1, \rho_R = 0.1$ and different system sizes L . Symbols stand for exact matrix computations, while solid (dashed) lines represent wAP (sAP) predictions. Convergence to the wAP prediction as L increases is apparent, similarly to the behavior observed for the KMP result in Fig. 2 of the main text.

confirmed in exact microscopic calculations, see Fig. 2. Moreover, data points for small L converge towards the wAP curve as L increases, very much like the results obtained for the KMP model of heat conduction, see Fig. 2 in the paper. This observation supports our analysis and conclusions for the KMP model, which strongly suggest that the weak additivity principle is indeed correct for sufficiently large system sizes.

To end this section, we apply the quantum Hamiltonian formalism to another stochastic lattice model, a fluid of random walkers [7]. The RW model can be seen as a variant of the ZRP with an interaction function $f(n) = n$. Such a linear interaction function implies that the probability for *each particle* to jump to a nearby site is independent of the population of the departure site, so particles behave as independent random walkers in $d = 2$. At the macroscopic level, the RW model is characterized by transport coefficients with components $D_\alpha(\rho) = h_\alpha$ and $\sigma_\alpha(\rho) = 2h_\alpha\rho$, so when coupled to boundary reservoirs at densities $\rho_{L,R}$ along the x -direction, with $\rho_L \neq \rho_R$, the RW fluid develops a linear stationary density profile

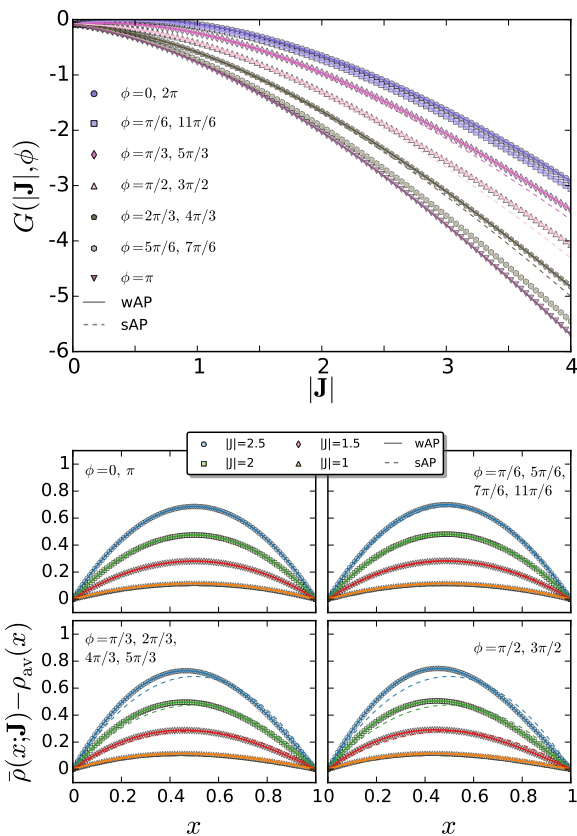


FIG. 3. (Color online) Top: Current LDF for the isotropic RW model ($h_x = 1/2, h_y = 1/2$) as a function of $|\mathbf{J}|$ for different angles $\phi = \tan^{-1}(J_y/J_x)$ and $\rho_L = 2, \rho_R = 1$. Bottom: Excess optimal density profiles for different $|\mathbf{J}|$ and ϕ . Symbols stand for exact matrix computations for $L = 10^5$, while solid (dashed) lines represent wAP (sAP) predictions.

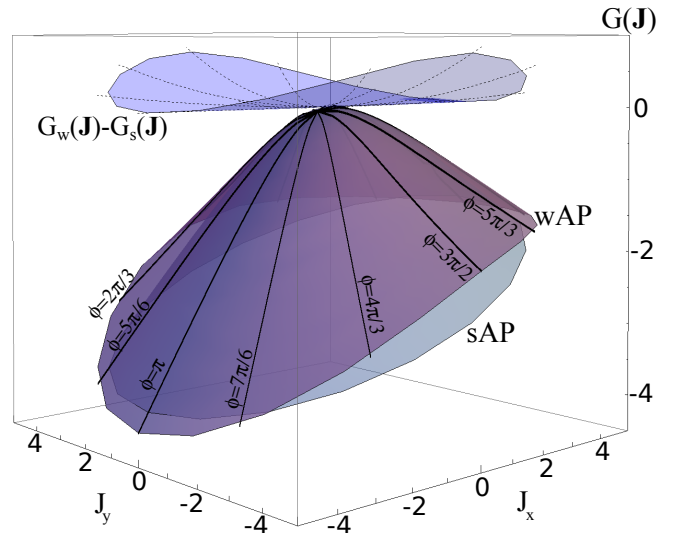


FIG. 4. (Color online) MFT predictions for the current LDF of the KMP model under both the wAP and sAP conjectures. Boundary densities for this plot are $\rho_L = 2$ and $\rho_R = 1$. Clearly, $G_w(\mathbf{J})$ lies above $G_s(\mathbf{J}) \forall \mathbf{J}$, except for current fluctuations along the gradient direction, $\mathbf{J} = (J_{\parallel}, 0) \forall J_{\parallel}$, where both solutions yield the same result, as demonstrated in the main text.

$\rho_{av}(x) = \rho_L + x(\rho_R - \rho_L)$ similar to that of the KMP model. Note however that the fluctuating behavior of both models is quite different because of their different mobilities. Fig. 3 shows our results for $G(\mathbf{J})$ (top) and $\bar{\rho}(x; \mathbf{J})$ (bottom) in the RW model, as obtained from the matrix method for $L = 10^5$ and compared with wAP and sAP theoretical results. Interestingly differences between wAP and sAP curves are not as pronounced as before (due to the relatively *weak* dependence of the transport coefficients on ρ for the RW model), but still the wAP offers correct predictions while the sAP fails for current fluctuations with components orthogonal to the gradient direction. All together, these results and those reported in the main text clearly demonstrate that the weak additivity principle yields the correct predictions for the current statistics of a broad class of d -dimensional interacting particle systems.

Finally, Fig. 4 displays the MFT prediction for the full current LDF of the 2d KMP model for $\rho_L = 2$ and $\rho_R = 1$ under both the wAP and sAP conjectures. Clearly the wAP current LDF improves over the sAP prediction for all current fluctuations, as proven in general in the main text on the basis of reverse Hölder's inequality.

-
- [1] R. Villavicencio and R.J. Harris, Local structure of current fluctuations in diffusive systems beyond one-dimension, *Phys. Rev. E* **93**, 032134 (2016).
- [2] G. M. Schütz. Exactly solvable models for many-body systems far from equilibrium. vol. 19 of *Phase Transitions and Critical Phenomena*, pages 1-251, Academic Press (2001).
- [3] P. Lloyd, A. Sudbury, and P. Donnelly, Quantum operators in classical probability theory: I. quantum spin techniques and the exclusion model of diffusion. *Stoch. Processes Appl.* **61** 205, (1996).
- [4] E. Levine, D. Mukamel, and G.M. Schütz, Zero-range process with open boundaries, *J. Stat. Phys.* **120**, 759 (2005).
- [5] R.J. Harris, A. Rakos, and G.M. Schütz, Current fluctuations in the zero-range process with open boundaries, *J. Stat. Mech.* P08003 (2005).
- [6] O. Hirschberg, D. Mukamel, and G.M. Schütz, Density profiles, dynamics, and condensation in the ZRP conditioned on an atypical current, *J. Stat. Mech.* P11023 (2015).
- [7] M. R. Evans, T. Hanney, Nonequilibrium Statistical Mechanics of the Zero-Range Process and Related Models, *J. Phys. A: Math. Gen.* **38** R195 (2005).
- [8] C. Kipnis, C. Marchioro and E. Presutti, Heat flow in an exactly solvable model, *J. Stat. Phys.* **27**, 65 (1982).
- [9] P.I. Hurtado, C. Pérez-Espigares, J.J. del Pozo, and P.L. Garrido, Thermodynamics of currents in nonequilibrium diffusive systems: theory and simulation, *J. Stat. Phys.* **154**, 214 (2014).
- [10] C. Giardinà, J. Kurchan and L. Peliti, Direct evaluation of large deviation functions, *Phys. Rev. Lett.* **96**, 120603 (2006).
- [11] V. Lecomte and J. Tailleur, A numerical approach to large deviations in continuous-time, *J. Stat. Mech.* P03004 (2007).
- [12] V. Lecomte and J. Tailleur, Simulation of large deviation functions using population dynamics, *AIP Conf. Proc.* **1091**, 212 (2009).
- [13] C. Giardinà, J. Kurchan, V. Lecomte and J. Tailleur, Simulating rare events in dynamical processes, *J. Stat. Phys.* **145**, 787 (2011).